ANALYSIS OF OPTICAL DIFFERENCES BETWEEN HEALTHY AND MALIGNANT OROPHARYNGEAL TISSUE USING AUTOFLUORESCENCE SIGNALS

Ruxandra Ioana STANCALIE-NEDELCU[1,2], Răzvan MIHALCEA[3], Șerban BERTESTEANU[1,2], Ionuț Relu ANDREI[3*], Adriana SMARANDACHE[3], Tatiana TOZAR[3], Raluca GRIGORE[1,2]

In the last years, there has been an increasing interest in the application of Laser Induced Autofluorescence (LIAF) as a noninvasive method for identifying alterations in biochemistry and tissue structure changes. Using a single case of oropharyngeal squamous cell carcinoma, we carried out an initial assessment to see if this method can show the differences between malignant and non-malignant tissue. The study focused on the application of the experimental methodology and preliminary comparative interpretation of the fluorescence response in healthy and malignant adjacent tissue and is not intended to statistically validate the technique. We developed and followed a standardized experimental protocol, adjusting technical factors such as excitation intensity, detection setup and sample thickness. The objective of this study is to evaluate the feasibility of the experimental methodology and to determine whether the observed optical differences sustain future studies involving larger patient cohorts.

Keywords: oropharyngeal cancer, optical diagnosis, LIAF;

1. Introduction

Oropharyngeal cancer represents a distinct subset of head and neck malignancies arising from the oropharynx, which anatomically includes the base of the tongue, palatine tonsils and tonsillar pillars, soft palate, and the posterior pharyngeal wall [1]. In recent decades, the epidemiology of oropharyngeal cancer has undergone significant changes, with an increasing incidence particularly attributed to human papillomavirus (HPV) related disease [2]. Traditionally, the development of oropharyngeal cancer has been strongly associated with well-established risk factors such as tobacco use and excessive alcohol consumption [3].

[1] Faculty of Medicine, "Carol Davila" University of Medicine and Pharmacy, 050474 Bucharest, Romania
[2] Department of ENT, Head and Neck Surgery, Colţea Clinical Hospital, 030167 Bucharest, Romania
[3] National Institute for Laser, Plasma and Radiation Physics, 409 Atomistilor St., RO-077125 Magurele, Romania
*Corresponding author: ionut.andrei@inflpr.ro

However, a growing proportion of cases are now linked to high-risk HPV infection, particularly HPV-16, which is recognized as a major etiological factor in oropharyngeal squamous cell carcinoma [4].

Oropharyngeal cancers are represented in most of the cases by squamous cell carcinomas (SCCs). Oral squamous cell carcinoma (OSCC) can be keratinizing and non-keratinizing SCCc [5]. Keratinizing SCCs are usually associated with chronic tobacco and alcohol consumption. They show keratin pearl formation, intercellular bridges, and marked cellular atypia. In contrast, non-keratinizing SCCs are often associated with high-risk HPV infection, especially HPV-16. Non-keratinizing SCCs display different morphological features, including basaloid cell populations, minimal keratinization, and increased mitotic activity [6].

Notably, HPV-positive oropharyngeal SCCs are now recognized as a distinct clinical and biological entity, often associated with better response to treatment and a favorable prognosis compared to HPV-negative SCCs [7].

The diagnosis of oropharyngeal cancer is made by performing a clinical examination and imaging investigations such as Computed Tomography (CT) and Magnetic Resonance Imaging (MRI). These are mandatory accompanied by endoscopy and confirmed by histopathological biopsy which is the gold standard in cancer diagnosis. Even if these medical examinations are essential for diagnosis and staging, they have also some limitations. Imaging techniques may have reduced sensitivity for detecting early mucosal changes and biopsy is an invasive method and may not fully capture the tumor heterogeneity [8,9,10].

Despite all the advances in diagnostic and therapeutic strategies, early detection and accurate characterization of malignant lesions remain challenging. This led to a major interest in auxiliary diagnostic approaches. Among these, optical techniques show particular promise. They may enable real-time, non-invasive assessment of changes in morphology and biological structure of the tissue [11].

Laser Induced Auto-Fluorescence (LIAF) is a non-invasive optical imaging method that showed encouraging potential in the diagnostic of oral cancer [12]. By detecting endogenous fluorescence signals in biological tissues, this technique can offer information about tissue changes. These changes appear at the level of the oropharyngeal mucosa [13]. Autofluorescence is stimulated by intrinsic fluorophores such as NADH, FAD, collagen, and elastin. Their concentration and distribution change during malignant transformation. These changes result in metabolic shifts, including increased proliferation and redox imbalance. They also indicate changes in the extracellular matrix. As a result, malignant tissue shows different autofluorescence patterns compared to healthy mucosa [14]. By visualizing these changes, LIAF enables real-time tissue characterization and aids in differentiating between healthy and malignant regions. Without altering the conventional diagnosis, this method can be a complementary tool, for guiding biopsies and enhancing the detection of early or subtle lesions [15].

Early detection of oropharyngeal cancer is important for improving patient survival and quality of life, as the patient's response to the treatment is more effective when the disease is identified at an early stage [16].

This study provides an overview of LIAF applications in oropharyngeal cancer. It includes a case-based analysis of a patient with oropharyngeal squamous cell carcinoma. The aim is to evaluate the ability of LIAF to detect differences in autofluorescence patterns between healthy and malignant tissue. Because the study was limited to a single patient case, the statistical analyses are presented as exploratory observations. They should not be considered representative of population-level conclusions. This work aims to encourage future research on non-invasive diagnostic approaches.

2. Materials and methods

The case presented in this study is about a 70 years old male known with a history of base of tongue carcinoma. He was previously treated with radiotherapy and chemotherapy. He presented in the ENT Department with findings suggestive of local recurrence. Clinical examination and CT-scan results indicated recurrent oropharyngeal disease. A biopsy was performed and confirmed a poorly differentiated, non-keratinizing basaloid squamous cell carcinoma with infiltrative and ulcerative features. Considering the patient's history, the current treatment consisted of salvage surgery represented by total laryngectomy extended to the base of the tongue, followed by adjuvant chemotherapy.

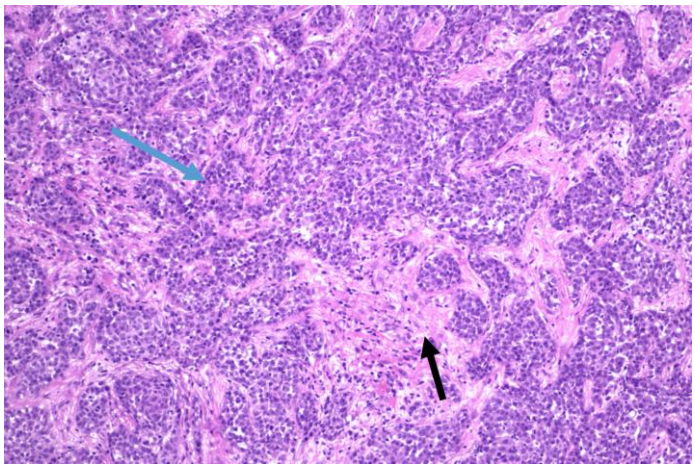


Fig. 1. Invasive squamous cells carcinoma (poorly differentiated) (low power field – x10): tumor showing infiltrative anastomosing cords (blue arrow) with loss of squamous maturation/architecture in a stroma with desmoplastic response (black arrow)

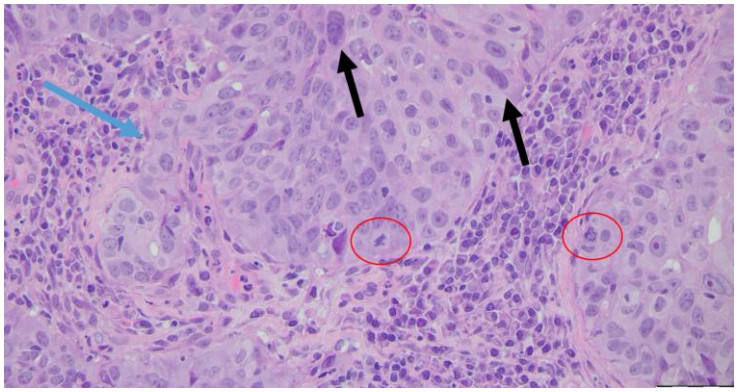


Fig.2. Invasive squamous cells carcinoma (poorly differentiated) (high power field - x40): tumor showing cells with marked nuclear pleomorphism (black arrow) and atypical mitoses (red circle); invasion into the stroma by a pushing border pattern of infiltration, occasionally with individual infiltrating cells (blue arrow); desmoplastic stroma with abundant lymphoplasmocytic inflammatory response

For this study, tissue samples were collected intraoperatively and transferred unfixed in order to preserve their optical properties. The tissue specimens were immediately cryopreserved. They were sectioned using a Laica cryostat at a thickness of 30 μm. Sections from the same specimen were prepared during the same cutting session to minimize thickness related variability. Paired samples were processed in the same manner. The samples were mounted unfixed and unstained on microscope slides. Samples showing necrosis or preparation artifacts such as folding and tissue fragmentation identified at microscope evaluation, were not considered in this study. All the samples were labeled and transported on dry ice to National Institute for Laser, Plasma, and Radiation Physics (INFLPR). They were analyzed within 24 hours, following a single freeze–thaw cycle to minimize the degradation effects.

LIAF measurements were made using an optical setup that involves controlled laser excitation and sensitive fluorescence detection, as shown in Fig. 3. We used a ps pulsed laser source at 375 nm (Alphals, PicoPower LD-375-50), operated at 31 MHz, 87 ps full width at half maximum, and 0.5 mW average power with the purpose to excite endogenous fluorophores (e.g., NADH, FAD. The laser beam of 1.6×1.8 mm spot was directed vertically onto the tissue surface, and a second mirror placed below the UV transparent substrate (1 mm thickness) reflected the transmitted beam to increase irradiation. The autofluorescence signal was collected through two optical fibers (Ocean Optics, M93L02 1500 μm) positioned at 45° angles by high sensitivity detectors such as photomultiplier module (Hamamatsu, H-6780-02) coupled with an oscilloscope (Tektronix, DPO7254 2.5 GHz), and a spectrograph (Acton Research, Spectra Pro SP2750) equipped with an

intensified - CCD camera (Princeton Instruments, PIMAX 1024) for lifetime and spectral analysis. To discriminate the LIAF signal from the scattered laser signal, a Log pass filter at 425 nm was used in the signal collection path for the photomultiplier. Laser and acquisition parameters were kept fixed to ensure reproducibility, and the automated XY linear translation stage was software controlled to perform a matrix-scan of the sample. The signals that were recorded were then processed to obtain fluorescence lifetime and spectra. Samples were scanned in a matrix with 2 mm spacing. The number of steps on OX and OY was adjusted to sample size for a uniform surface coverage (Fig. 3, inset). Signals were collected from up to 22 points and each averaged over 200 laser pulses. Signal acquisition was synchronized through a TTL signal from the laser diode driver. The acquired data were processed with dedicated software and used to analyze lifetime, and intensity and spectral variations allowing identification of tumoral (T) and healthy (H) tissue differences, and suggesting the use of LIAF as a tool for optical tissue evaluation [13, 17].

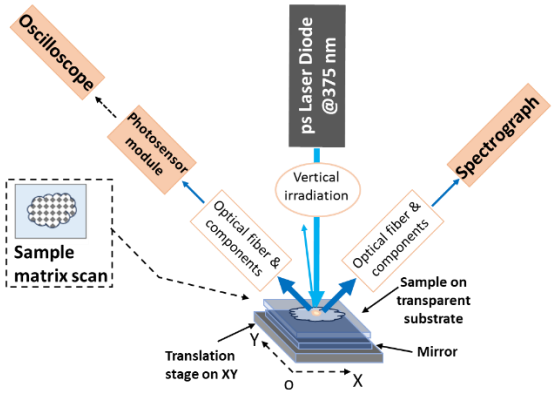


Fig.3. Setup of spectral and lifetime investigation of the tissue autofluorescence using a double-pass laser beam irradiation geometry and signal acquisition at 45°; the inset, schematic representation of matrix scan.

3. Results

Two healthy (H1, H2) and two tumoral (T1, T2) tissue samples were collected and studied. LIAF spectra were obtained in real time for all samples. Improving the discrimination between the two types of tissues was possible by averaging multiple individual spectra.

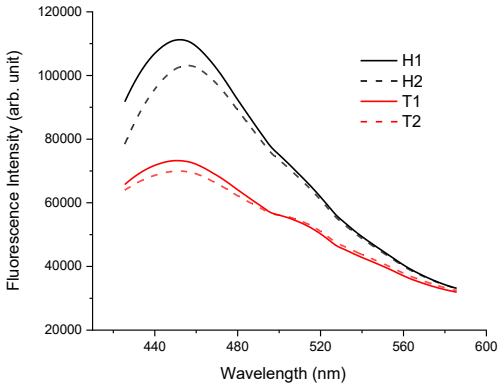


Fig. 4. Average autofluorescence intensity for tumoral (T) and healthy (H) tissues, each with two replicates (1 and 2).

The two LIAF spectra, respectively healthy (H1) and malignant (T1), show a similar profile, with a broad emission band with maximums at 450–460 nm as it can be observed in Fig. 4. The healthy samples exhibit higher fluorescence intensity, especially near the main peak. This emphasizes changes in the endogenous fluorophores and tissue microstructure. The clear spectral separation in the blue and green regions supports the potential of LIAF as an optical method for tissue discrimination.

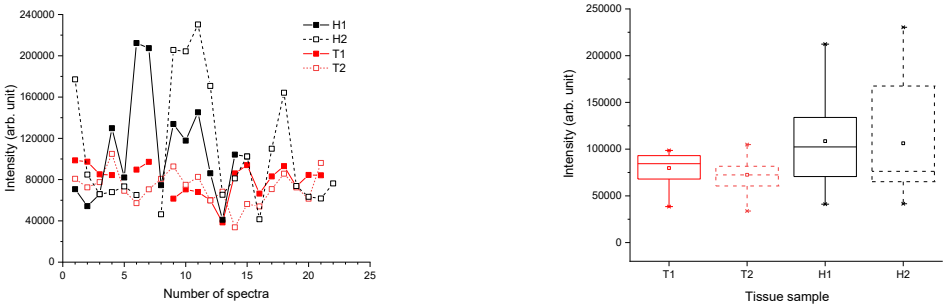


Fig. 5. Distribution of (a) fluorescence intensity for individual spectra during matrix scan of the sample, and (b) average autofluorescence intensity for T and H tissues samples.

Point-by-point sample scanning for fluorescence intensity analysis shows a consistent distinction between non-malignant (H1) and malignant (T1) tissues as illustrated in Fig.5 (a). In most spectra, healthy samples display higher intensity values than malignant ones. Both tissue types exhibit variability in fluorescence intensity, but healthy samples tend to show higher peak values and greater dispersion. Several healthy spectra reach markedly elevated intensities, while

malignant measurements remain within a lower range. This supports the averaged analysis, confirming that the differences are also present at the level of individual spectra.

The box-plot in Fig. 5(b) shows the distribution of autofluorescence intensities for H1 and T1 tissues. Healthy samples have a higher median intensity and a wider interquartile range, indicating both increased signal and greater variability. In contrast, malignant tissue exhibits lower, more consistent intensity values.

Table 1

Statistical comparison of the fluorescence intensity for T1, H1

Tukey Test								
	Mean Diff	SEM	q Value	Prob	Alpha	Sig	LCL	UCL
Intensity	39078.78318	11971.27544	4.61653	0.00216	0.05	1	14936.36165	63221.20471
Fisher Test								
	Mean Diff	SEM	T Value	Prob	Alpha	Sig	LCL	UCL
Intensity	39078.78318	11971.27544	3.26438	0.00216	0.05	1	14936.40539	63221.16097

As represented in table 1, the statistical analysis, Tukey and Fisher tests, revealed a significant difference in fluorescence intensity between H1 and T1 tissues. The mean difference was approximately 39,078 ± 11,971 (SEM), with both tests yielding $p = 0.00216$, confirming statistical significance at $\alpha = 0.05$. The 95% confidence interval (≈14,936 to 63,221) excludes zero, indicating that the observed difference is unlikely due to random variation.

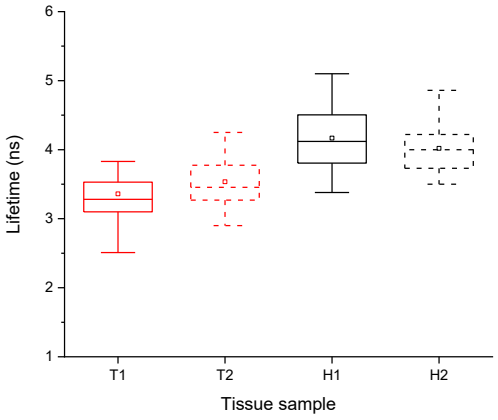


Fig.6. Distribution of average fluorescence lifetime for T and H tissues samples for the two replicates.

The box-plot representation of fluorescence lifetime measurements reveals a clear distinction between T1 and H1 tissue samples as in Fig.6. The non-malignant tissue exhibits a noticeably higher median fluorescence lifetime compared to the malignant tissue, indicating a systematic decrease in excited-state decay times associated with malignant transformation.

Table 2

Statistical analysis of fluorescence lifetime measurements for T1, H1- Overall ANOVA

	DF	Sum of Squares	Mean square	F Value	Prob>F
Model	1	9.85288	9.85288	9.28999	0.00402
Error	41	43.48423	1.06059		
Total	42	53.33712			

Table 3

Statistical analysis of fluorescence lifetime measurements for T1, H1- Tukey Test

	Mean Diff	SEM	q Value	Prob	Alpha	Sig	LCL	UCL
Lifetime	0.97905	0.32122	4.31045	0.00402	0.05	1	0.33034	1.62776

Table 4

Statistical analysis of fluorescence lifetime measurements for T1, H1- Fisher Test

	Mean Diff	SEM	T Value	Prob	Alpha	Sig	LCL	UCL
Lifetime	0.97905	0.32122	3.04795	0.00402	0.05	1	0.33034	1.62776

Statistical analysis of fluorescence lifetime reveals a significant difference between T1 and H1 tissues. The overall ANOVA method indicates that this effect is significant, by demonstrating that the null hypothesis of equal means as in table two can be rejected. Post-hoc tests confirm the result as seen in tables three and four: Tukey (mean difference $\approx 0.979 \pm 0.321$, $p = 0.00402$) and Fisher ($t = 3.05$, $p = 0.00402$).

The averaged LIAF spectra for H2, represented by the black curve, respectively T2, depicted with the red curve, reveal clear differences in fluorescence intensity across the investigated wavelength range. This can be observed in Fig. 4. Both tissue types exhibit a broad emission band with maximum intensities around 450–460 nm, followed by a progressive decrease in fluorescence intensity toward longer wavelengths.

Point-by-point sample scanning in the Fig. 5(a) corresponding to the second replicate shows independent patterns between T2 and H2 tissues, with higher degrees of changes than in the first case. Healthy samples exhibit pronounced variations and higher intensity peaks. In contrast, malignant tissue displays lower, more stable, and tightly clustered intensity values. Despite some overlap, healthy tissue generally shows higher maxima and greater variability.

The box-plot analysis of fluorescence intensity in the Fig. 5(b) for the second replicate reveals differences between T2 and H2 tissue samples. The healthy tissue shows a higher median fluorescence intensity compared to the malignant tissue, indicating a decrease in autofluorescence associated with tumor presence.

Table 5

Statistical comparison of the fluorescence intensity for T2, H2

Tukey Test								
	Mean Diff	SEM	Q Value	Prob	Alpha	Sig	LCL	UCL
Intensity	32144.63471	13487.95661	3.37037	0.02176	0.05	1	4924.79092	59364.47851
Fisher Test								
	Mean Diff	SEM	T Value	Prob	Alpha	Sig	LCL	UCL
Intensity	32144.63471	13487.95661	2.38321	0.02176	0.05	14924.83627	4924.83627	59364.43315

Statistical analysis of the second replicate shows a significant difference in fluorescence intensity between malignant and non-malignant tissues, with higher mean values in healthy samples. Post-hoc tests confirm this as shown in table 5: Tukey (mean difference ≈ 32,145 ± 13,488; $p = 0.02176$) and Fisher ($t = 2.38$; $p = 0.02176$). At $\alpha = 0.05$, the difference is statistically significant.

The box-plot representation of fluorescence lifetime measurements for the second replicate in the Fig. 6 reveals differences between H2 and T2 tissue samples. The malignant tissue exhibits a lower median fluorescence lifetime compared to the non-malignant tissue.

Table 6

Statistical analysis of fluorescence lifetime measurements for T2, H2- Overall ANOVA

	DF	Sum of square	Mean square	F Value	Prob>F
Model	1	3.47384	3.47384	15.41176	3.23531
Error	41	9.24148	0.2254		
Total	42	12.71532			

Table 7

Statistical analysis of fluorescence lifetime measurements for T2, H2- Tukey Test

	Mean Diff	SEM	q Value	Prob	Alpha	Sig	LCL	UCL
Lifetime	0.56861	0.14484	5.55189	3.23606	0.05	1	0.2761	0.86113

Table 8

Statistical analysis of fluorescence lifetime measurements for T2, H2- Fisher Test

	Mean Diff	SEM	T Value	Prob	Alpha	Sig	LCL	UCL
Lifetime	0.56861	0.14484	3.92578	3.23531	0.05	1	0.2761	0.86113

Statistical analysis of fluorescence lifetime in the second replicate reveals differences between malignant and non-malignant tissues. One-way ANOVA confirms this effect ($F = 15.41$, $p = 3.24 \times 10^{-4}$) that can be seen in the table 6. Post hoc tests support the result as in the tables 7 and 8: Tukey (mean difference $\approx 0.57 \pm 0.145$; $p = 3.24 \times 10^{-4}$) and Fisher ($t = 3.93$; $p = 3.24 \times 10^{-4}$).

4. Conclusions

The present study represents a subsequent stage of the research previously reported in [13], extending the investigation of laser-induced autofluorescence (LIAF) in upper aerodigestive tract malignancies to a new clinical case of oropharyngeal squamous cell carcinoma. The purpose of including this additional case was to evaluate whether the optical differences observed previously between malignant and non-malignant tissues could also be identified under similar experimental conditions in an independent sample. The results obtained are consistent with the findings reported in the previous work, showing comparable variations in autofluorescence intensity and fluorescence lifetime between healthy and tumoral tissues. Preliminary differences in fluorescence response were observed between the investigated paired tissue types. These findings suggest that malignant tissue is associated with reduced autofluorescence intensity compared to healthy tissue, reflecting biochemical and structural alterations occurring during tumor transformation. The present investigation was limited to a single patient case and was not intended to establish statistically validated diagnostic criteria or clinical application. The main purpose of the study was to evaluate the experimental methodology and to figure if the observed optical behavior justifies further studies in larger patient cohorts. Overall, while preliminary, the results of this study suggest that LIAF may represent a promising approach for supporting the evaluation of malignant and non-malignant oropharyngeal tissues. Future studies involving additional samples will be necessary to further assess the reproducibility and potential relevance of the proposed approach.

Acknowledgements

This research was funded by Romanian Ministry of Education and Research, National Research Authority and UEFSCDI [grant numbers PN-IV-P7-7.1-PED-2024-1995 and PN-IV-P2-2.1-TE-2023-1686]; the Romanian National Program LAPLAS VII [grant number 30N/2023]; the PNCDI IV and IFA ELI-RO Program [grant numbers ELI-RO/RDI/2024_022_RAY-PDT and LI-RO/RDI/DEZ/DFG/2025_024].

The study was conducted in accordance with the Declaration of Helsinki and approved by the Institutional Ethics Committee of Coltea ENT Clinic- Hospital in Bucharest (protocol code 5323/obcc and 20.03.2023).

R E F E R E N C E S

[1] *H.J. Hoekstra, T. Wobbes, E. Heineman, S.Haryono, T. Aryandono, C. Balch*, Fighting global disparities in cancer care: a surgical oncology view, Ann Surg Oncol, Vol. 23, 2131–2136, 2016.

[2] *J. Ferlay, I. Soerjomataram, M. Ervik, R. Dikshit, S. Eser, C. Mathers,* Cancer Incidence and Mortality Worldwide: IARC CancerBase, GLOBOCAN v1.0, No. 11, 2013.

[3] *J.L. Ferreira Antunes, T.N. Toporcov, M.G.H. Biazevic, A.F. Boing, C. Scully, S. Petti,* Joint and Independent Effects of Alcohol Drinking and Tobacco smoking on Oral Cancer: a Large Case-Control Study, PLoS One, 8, Article e68132, 2013.

[4] *K. Ang, J. Harris, R. Wheeler, R. Weber, D. Rosenthal, et. al,* Human papillomavirus and survival of patients with oropharyngeal cancer, New England Journal of Medicine, 363(1), 24–35, 2010.

[5] *J. Crissman, D. Gnepp, M. Goodman, M. Hellquist, M. Johns,* Preinvasive lesions of the upper aerodigestive tract: histologic definitions and clinical implications (a symposium), Pathol Annu, 22 Pt 1:311-52. PMID: 3574982, 1987.

[6] *W. Sakr, R. Zarbo, J. Jacobs, J. Crissman,* Distribution of basement membrane in squamous cell carcinoma of the head and neck, Hum Pathol, 18(10):1043-50, 1987.

[7] *J. Lewis,* Immunohistochemistry as a standalone test for risk stratification in oropharyngeal squamous cell carcinoma, Head and Neck Pathology, 6(Suppl 1), S75–S82, 2012.

[8] *A. Weber, L. Romo, S. Hashimi,* Malignant tumors of the oral cavity and oropharynx: clinical, pathologic, and radiologic evaluation. Neuroimaging Clin N Am, 13:443–464, 2003.

[9] *A. Zima, J. Wesolowski, M. Ibrahim, et al.,* Magnetic resonance imaging of oropharyngeal cancer, Top Magn Reson Imaging, 18:237– 242, 2007.

[10] *D. Nair, R. Pruthy, U. Pawar, P. Chaturvedi,* Oral cancer: Premalignant conditions and screening – An update. J Cancer Res Ther., 8(Suppl 1), S57–66, 2012.

[11] *T. Stefanescu, I. Gruia, I.M. Gruia, C. Motoc,* Correlation of optical methods and biochemical measurements for investigation membrane changes of normal and malign tissues, U.P.B. Sci. Bull., Series A, Vol. 72, Iss. 1, ISSN 1223-7027, 2010.

[12] *Y. Yan, T.Huang, N. Cheng, Y. Hsieh, M. Tsai, J. Chiou, J. Duann, Y. Lin, C. Yang, M. Ou-Yang,* Portable LED-induced autofluorescence spectroscopy for oral cancer diagnosis, J. Biomed. Opt, 22, 045007, 2017.

[13] *R. Stăncălie-Nedelcu; S. Berteșteanu; G. Bertesteanu; I. Andrei; A. Smarandache; A. Staicu; T. Tozar; R. Costin; R. Grigore;* Exploratory Approach Using Laser-Induced

Autofluorescence for Upper Aerodigestive Tract Cancer Diagnosis—Three Case Reports. Appl. Sci., 16, 1536, 2026.

[14] *J. Lagarto, B. Dyer, C. Talbot, N. Peters, P. French, A. Lyon, C. Dunsby,* Characterization of NAD(P)H and FAD autofluorescence signatures in a Langendorff isolated-perfused rat heart model. Biomed Opt Express, 9(10):4961-4978, 2012.

[15] *R. Mallia, S. Thomas, A. Mathews, R. Kumar, P. Sebastian, J. Madhavan, et al.,* Laser-induced autofluorescence spectral ratio reference standard for early discrimination of oral cancer. Cancer, 112:1503–12, 2018.

[16] *A. Singh,* Contemporary insights into head and neck cancers: Epidemiology, molecular biology, diagnosis, and therapeutic advances, Cancer Treatment and Research Communications, Volume 46, 101086, ISSN 2468-2942, 2026.

[17] *T. Tozar, I. Andrei, R. Costin, M. Pascu, R. Pirvulescu,* Laser induced autofluorescence lifetime to identify larynx squamous cell carcinoma: Short series ex vivo study, Journal of Photochemistry and Photobiology B: Biology, Volume 202, 111724, 2020.